Nano Research
2023, 16(1): 1269–1276

ISSN 1998-0124 CN 11-5974/O4
https://doi.org/10.1007/s12274-022-4766-8

Research Article

A self-powered piezoelectret sensor based on foamed plastic garbage for monitoring human motions

Yujun Shi[1], Kaijun Zhang[1], Sen Ding[2], Zhaoyang Li[1], Yuhao Huang[1], Yucong Pi[1], Dazhe Zhao[1], Yaowen Zhang[1], Renkun Wang[1], Binpu Zhou[2], Zhi-Xin Yang[3] (✉), and Junwen Zhong[1] (✉)

[1] *Department of Electromechanical Engineering and Centre for Artificial Intelligence and Robotics, University of Macau, Macau 999078, China*
[2] *Joint Key Laboratory of the Ministry of Education, Institute of Applied Physics and Materials Engineering, University of Macau, Avenida da Universidade, Macau 999078, China*
[3] *State Key Laboratory of Internet of Things for Smart City and Department of Electromechanical Engineering, University of Macau, Macau 999078, China*

Received: 12 April 2022 / **Revised:** 21 June 2022 / **Accepted:** 12 July 2022

ABSTRACT

Constructing piezoelectret based on foamed plastic garbage is an advisable strategy for obtaining self-powered flexible electromechanical sensors with good performances. Herein, a self-powered piezoelectret sensor with basic material of low density polyethylene (LDPE) foamed plastic garbage is proposed, with characteristics of easy fabrication, excellent flexibility, and high equivalent piezoelectric coefficient d_{33} value up to ~ 1,100 pC/N. The output stability is verified by continuously stimulating a sensor for ~ 180,000 cycles under low and high applied pressure, and the variations of peak outputs are less than 5.5%. Applications for measuring low- and high-pressure signals from human body are achieved. Assembled with a wristband, a sensor is demonstrated for detecting the human pulse waves. Moreover, real time human sitting information is wirelessly monitored with a smart chair based on 4 pixels sensors array.

KEYWORDS

wearable electronics, piezoelectret, self-powered, pressure sensor, mobile health

1 Introduction

The use of plastics now is pervasive in every corner of daily life and the plastic garbage problem has become a serious problem [1–3]. In specific, with the fast development of logistics transportation in recent years, the packaging garbage made of foamed plastics is widely used [1, 2, 4]. For instance, it's reported that Amazon's plastic packaging garbage soared to 270,000 tons in 2020 [5]. The main structures of macroscopic air bubbles inside the foamed plastics endow the characteristics of light weight and good flexibility/softness [4, 6]. The basic structure of foamed plastics is the same as a kind of artificial flexible piezoelectric materials called "piezoelectret" [7–12]. Piezoelectret exhibits strong piezoelectricity after electric charging to generate electrostatic charges inside the air bubble structures as the macroscopic electrical dipoles. When mechanically stimulated, the thickness of piezoelectret changes, thus changing the moments of the electrical dipoles. As a result, mechanical signals are converted into electrical ones [12, 13]. Similar to other flexile self-powered sensors based on traditional piezoelectric polymers [14–17] and triboelectric sensors (especially some fabric triboelectric sensors) [18–29], flexible piezoelectret sensors have features of sensitive to dynamic stimuli, good output stability, and low modulus of elasticity [8, 12, 30–32], etc. Furthermore, benefitting from the high equivalent d_{33} coefficients, flexible piezoelectret sensors have been demonstrated with wide applications in sensing various electromechanical signals from human body, such as pulse waves, joint or muscle movement, breath information, and so on [13, 31–36]. There is no doubt that converting the ordinary foamed plastic garbage into the piezoelectret materials with excellent electromechanical conversion properties via an easy fabrication technology is an advisable strategy to realize the concept of "turning garbage into treasure".

Low density polyethylene (LDPE) foamed plastic is one of the most common packaging garbage [4]. In this work, the inner air bubble structures of the LDPE foamed plastic are coated with a thin layer of Teflon amorphous fluoropolymer (AF) electret [37] to form the LDPE/Teflon AF piezoelectret with good flexibility and strong piezoelectricity. Flexible self-powered electromechanical sensors based on LDPE/Teflon AF piezoelectret are fabricated for monitoring human motions and several important features are achieved: (i) The equivalent piezoelectric coefficient d_{33} value is up to ~ 1,100 pC/N; (ii) the variations of output stability under low and high applied pressure are less than 5.5% when a sensor continuously works for ~ 180,000 cycles; (iii) to demonstrate low pressure detection, a sensor is assembled with a wristband for detecting the frequency and typical characteristics of human pulse waves; (iv) to demonstrate high pressure detection, a smart chair based on 4 pixels sensors array wirelessly monitors various human sitting information in real time.

Address correspondence to Zhi-Xin Yang, zxyang@um.edu.mo; Junwen Zhong, junwenzhong@um.edu.mo

2 Results and discussion

2.1 Fabrication of the self-powered piezoelectret sensor with basic material of LDPE foamed plastic garbage

Figure 1(a) shows the schematic diagram of the self-powered piezoelectret sensor. It mainly consists of two Al electrodes sandwiching a piece of LDPE/Teflon AF piezoelectret, with detailed fabrication process of the sensor illustrated in Fig. S1 in the Electronic Supplementary Material (ESM). Air bubble structures are naturally existing inside the LDPE foamed plastic and Teflon AF can penetrate into the air bubbles and deposit on the inner surfaces after a spin-coating and then curing process. As a result, LDPE/Teflon AF piezoelectret was formed with such an easy fabrication process. Teflon AF is an excellent electret material that can stably hold high electrostatic charge density because of containing rich Fluorine element [38]. After the fabricated piezoelectret is polarized by Corona charging method, the Teflon AF layers can capture electrostatic charges to generate the macroscopic electrical dipoles, which endows the material with piezoelectricity. The macroscopic electrical dipoles will also induce charges in Al electrodes (50 μm-thick Al tape) adhered on two outer surfaces. Figure 1(b) shows the cross-section view scanning electron microscopy (SEM) image of the LDPE/Teflon AF piezoelectret, indicating that air bubble structures remain after the fabrication process and the material thickness is around 600 μm. The enlarged SEM image in Fig. 1(c) and corresponding energy-dispersed X-ray spectrum (EDS) image in Fig. 1(d) of LDPE/Teflon AF piezoelectret prove that Teflon AF is successfully coated on the inner surfaces of the air bubble, as abundant Fluorine element exists. Very few Fluorine element is found in the EDS for LDPE raw material (Fig. S2 in the ESM). Figure 1(e) shows the photo of the fabricated sensor with effective size of 2 cm × 2 cm and the total weight is only 90 mg (Fig. S3 in the ESM). The LDPE foamed plastic as raw material is from the packaging garbage that is used for packing computer monitors (Fig. 1(f)), and only 200 μL of 3 wt.% Teflon AF solution is used in the fabrication, and thus the cost of our sensor is low. Figure 1(g) demonstrates the flexibility the sensor, which can be easily twisted to 60° by fingers.

Figure 1(h) shows the long-term measured piezoelectric coefficients of a sensor with size of 2 cm × 2 cm, which is defined as equivalent d_{33}. The equivalent d_{33} values drop quickly in the first week and then maintain roughly stable in the following weeks. The equivalent d_{33} values are measured via a "weight moving method" [32, 33] which is normally used to measure quasi-static d_{33}, as shown in Fig. S4 in the ESM. Figure 1(i) shows the generated output current versus time curve when moving a weight with gravity of 1 N and the corresponding transferred charge versus time curve. Equivalent d_{33} = transferred charge (Q)/weight gravity (F), and the equivalent d_{33} value for the 8th testing week is ~ 1,100 pC/N. With similar size, the equivalent d_{33} value of a sensor based on traditional cellular polypropylene piezoelectret is about 600 pC/N [32, 33].

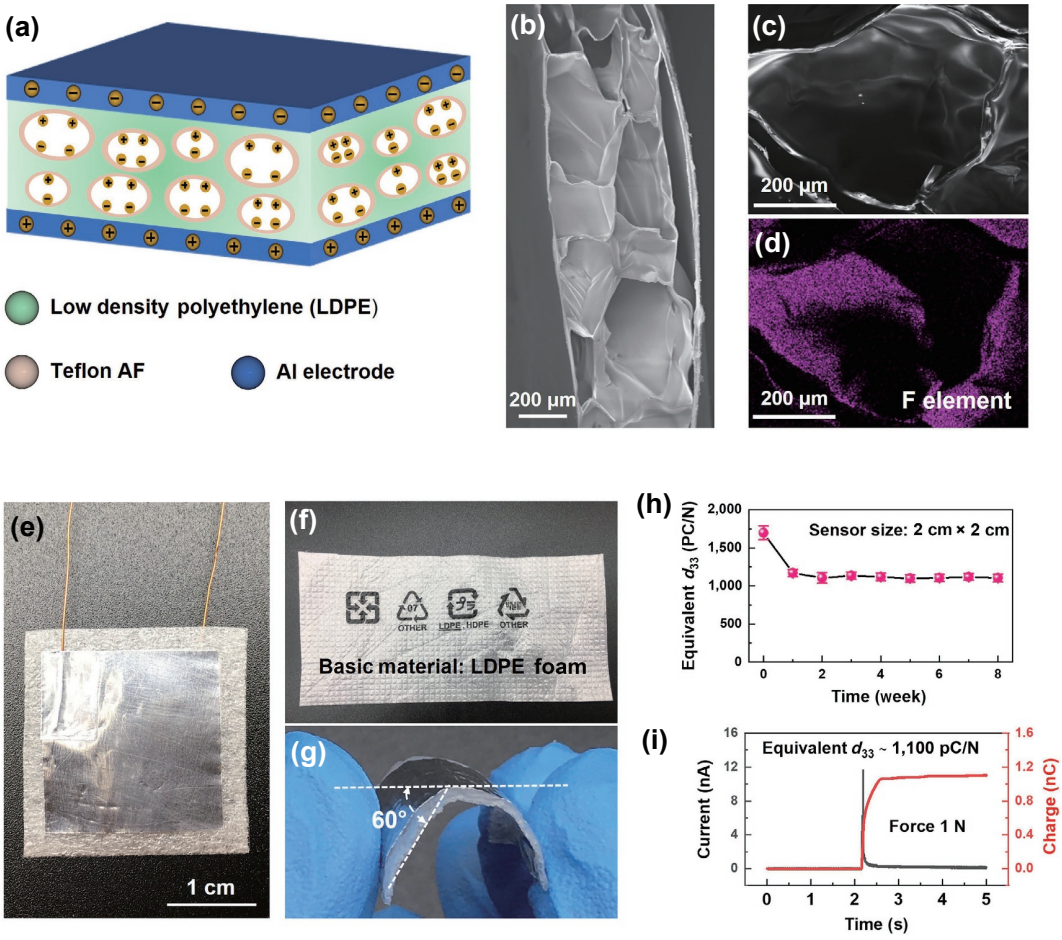

Figure 1 Design of the self-powered sensor based on LDPE/Teflon AF piezoelectret. (a) Schematic diagram illustrating the structure of the sensor. (b) Cross-sectional SEM image of the LDPE/Teflon AF piezoelectret. (c) Enlarged SEM image and (d) corresponding EDS image of the LDPE/Teflon AF piezoelectret. (e) Photo of a fabricated sensor with size of 2 cm × 2 cm. (f) Photo of the LDPE foamed plastic raw material. (g) Photo illustrating the flexibility of the sensor. (h) Long-term equivalent piezoelectric coefficient d_{33} values versus time curves for a sensor with size of 2 cm × 2 cm. (i) Output current versus time curve and corresponding transferred charges for the 8th testing week, when moving a weight with gravity of 1 N.

2.2 Working mechanism and key parameters affecting the output performances

Figure 2(a) shows the working mechanism of the self-powered piezoelectret sensor. By pressing and releasing the sensor, the thickness of air bubble structure and the dipole moment of the macroscopic electrical dipoles are changed to break the balance of the electrical potential between the two Al electrodes. The unbalanced electrical potential will drive the current flow through the external load. As a result, alternative mechanical signal is converted into AC electrical outputs. In general, the basic working mechanism of piezoelectret sensors and triboelectric sensors is the same, which is the electrostatic induction effect caused by the electrostatic charges inside the devices [21, 30]. However, the electrostatic charges of triboelectric sensors are mainly generated by the triboelectric effect, while the electrostatic charges of piezoelectret sensors are mainly generated by Corona charging process. Moreover, under pressing and releasing a sensor with external load of 20 MΩ by hand, switching polarity tests in Fig. 2(b) indicates that the electric signal is generated from the sensor rather than from the measurement system [31].

LDPE foamed plastic samples with and without coating with Teflon AF are Corona charged with the setup in Fig. S5 in the ESM with charging voltage of up to −15 kV and charging time of 5 min. The surface potential values of the samples can be measured by an electrostatic voltmeter in Fig. S6 in the ESM. Under the same size of 2 cm × 2 cm, the surface potential versus time curves of LDPE with and without Teflon AF are shown in Fig. 2(c). Just after polarization, the initial surface potential of LDPE without Teflon AF is higher than that of LDPE with Teflon AF. However, LDPE without Teflon AF cannot hold this high potential and drops to average potential of ~ −3 V after 48 h, and

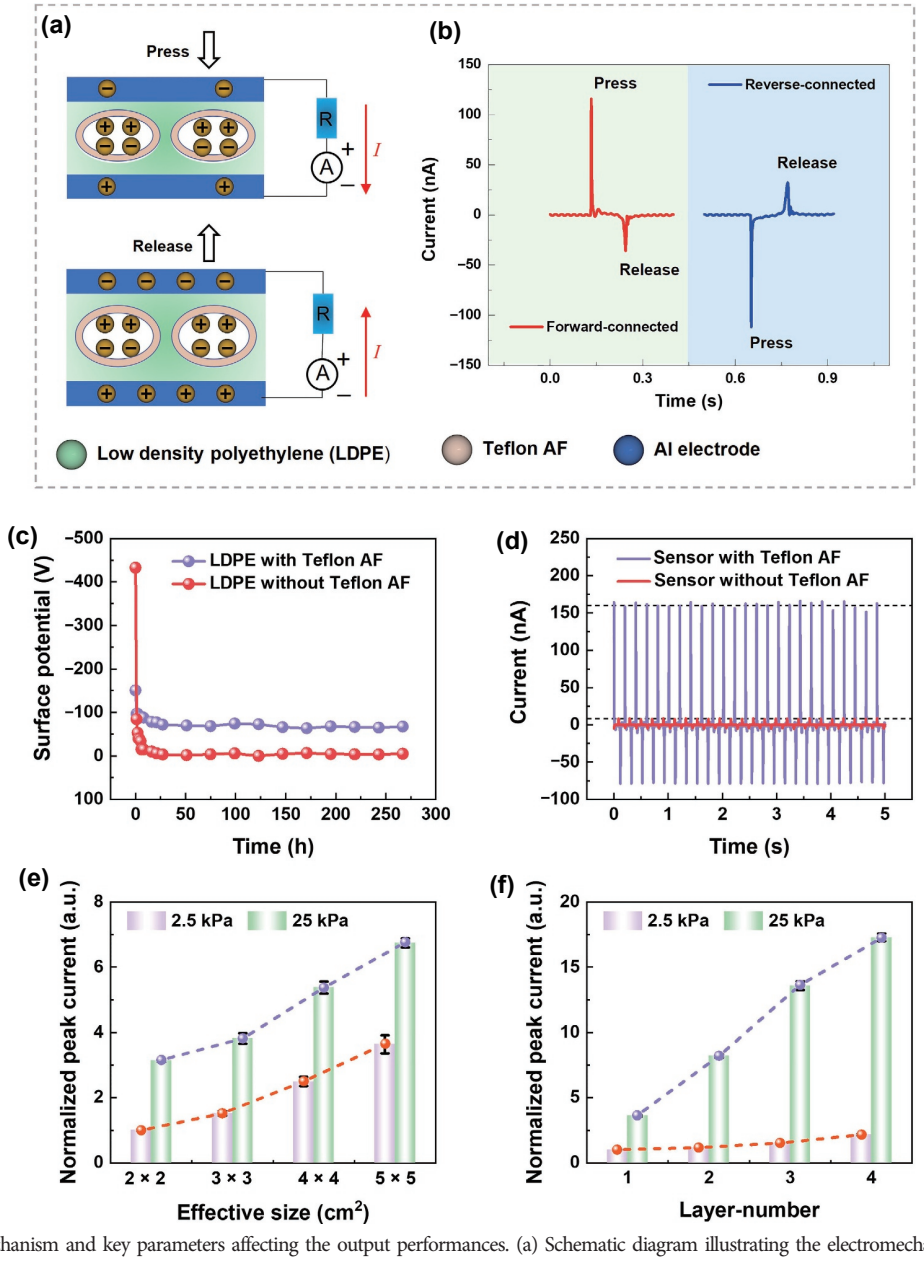

Figure 2 Working mechanism and key parameters affecting the output performances. (a) Schematic diagram illustrating the electromechanical signals converting process of the sensor, under pressing and releasing motions. (b) Output current versus time curves for a sensor with forward and reverse connection to the measuring system, with an external load of 20 MΩ. (c) Surface potential versus time curves for LDPE with and without Teflon AF. (d) Output current for sensors based on LDPE with and without Teflon AF, under applied pressure of 25 kPa, frequency of 5 Hz, and load resistance of 40 MΩ. (e) Normalized peak currents under both low (2.5 kPa) and high (25 kPa) applied pressure for sensors with effective size of 2 cm × 2 cm, 3 cm × 3 cm, 4 cm × 4 cm, and 5 cm × 5 cm, under frequency of 5 Hz. (f) Normalized peak currents under both low (2.5 kPa) and high (25 kPa) applied pressure for sensors with 1-layer, 2-layers, 3-layers, and 4-layers of piezoelectret, under frequency of 5 Hz.

then remains at such low value in the following testing time. The surface potential of LDPE with Teflon AF also quickly decreases in the first 48 h and then keeps the average potential at ~ −68 V until the testing time of ~ 265 h. On the other hand, under applied pressure of 25 kPa, frequency of 5 Hz, and load resistance of 40 MΩ, the peak output current values of sensors based on LDPE with and without Teflon AF are measured with a testing system in Fig. S7 and Table S1 in the ESM. The peak output current values for two devices are ~ 160 and ~ 8 nA, respectively, as shown in Fig. 2(d). The above results indicate that LDPE foamed plastic works as framework and Teflon AF acts as key electrostatic holding materials in the LDPE/Teflon AF piezoelectret.

The effective size is also an important factor which will affect the output performance of the sensor. Sensors with effective size of 2 cm × 2 cm, 3 cm × 3 cm, 4 cm × 4 cm, and 5 cm × 5 cm were fabricated as shown in Fig. S8 in the ESM. The average amount of Teflon AF is the same for sensors with different sizes, which is 50 μL/cm^2. When the above four sensors are connected to an external resistance of 40 MΩ and the frequency is fixed at 5 Hz, the normalized peak currents under both low (2.5 kPa) and high (25 kPa) applied pressure are compared in Fig. 2(e). Apparently, regardless of the high and low pressures, the normalized peak currents show an increasing trend with the increase of effective size. Moreover, the influence of the layer-number of LDPE/Teflon AF piezoelectret is studied. As shown in Fig. S9 in the ESM, sensors with 1-layer, 2-layers, 3-layers, and 4-layers of LDPE/Teflon AF piezoelectret were fabricated. It is worth noting that when the layer-number is greater than 1, we first glue the LDPE/Teflon AF piezoelectret together one layer by one layer, and then polarize it as a whole by means of Corona charging, and the polarization conditions are the same as those in Fig. S5 in the ESM. Under the same effective size of 2 cm × 2 cm, the normalized peak currents under 2.5 and 25 kPa of above four sensors are compared in Fig. 2(f), with frequency of 5 Hz. Clearly, the normalized peak currents tend to increase with the increasing layer-number of LDPE/Teflon AF piezoelectret for both high and low pressures. However, increasing the layer numbers will hamper the flexibility, and sensors with 1-layer piezoelectret are used for the following test and demonstration.

2.3 Systematic output characterization

The testing system in Fig. S7 and Table S1 in the ESM is still employed to systematically characterize the output performance of a sensor with 1-layer of LDPE/Teflon AF piezoelectret and effective size of 2 cm × 2 cm. When the sensor is connected to a resistance of 40 MΩ under a fixed frequency of 5 Hz, the load current versus time curves under different applied pressure are illustrated in Fig. S10 in the ESM and the peak current versus applied pressure curve is plotted in Fig. 3(a). The sensor exhibits good linear output in both low-pressure and high-pressure regions and the curve shows that two regions have different sensitivities. The sensitivity of high-pressure region (2.5–50 kPa) is lower than that of low-pressure region (≤ 2.5 kPa), with corresponding sensitivities of 2.62 and 20.73 nA/kPa, respectively. These observations are similar to those of other sensors based on piezoelectret materials [32, 33]. Under respective applied pressure of 2.5 and 25 kPa, the performances under various frequencies are shown in Fig. 3(b). The peak current increases approximately linearly with the increasing frequency from 2 to 8 Hz for both applied pressures, which also matches the performance of reported piezoelectret sensor [33].

The long-term output stability is very important for sensors, which matters their practicality. In order to evaluate the stability of the sensor under low (2.5 kPa) and high (25 kPa) pressure, the sensor is continuously stimulated at 5 Hz when it is connected to a resistance of 40 MΩ. The sensor continuously works for 10 h under each pressure, with total working cycles of up to ~ 180,000. 1 min of current versus time curves are measured for each testing hour and the results under two applied pressures are shown in Figs. 3(c) and 3(d). To quantitatively assess the variation of peak

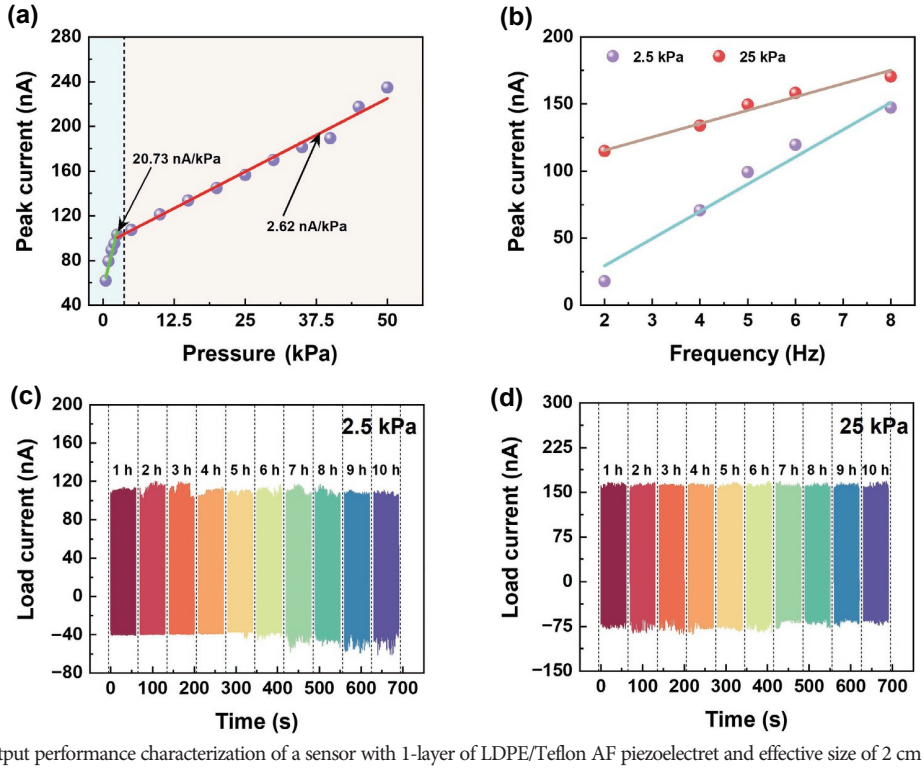

Figure 3 Systematic output performance characterization of a sensor with 1-layer of LDPE/Teflon AF piezoelectret and effective size of 2 cm × 2 cm. (a) Peak current versus applied pressure curve, under load resistance of 40 MΩ and frequency of 5 Hz. (b) Peak current versus frequency curves when the sensor is connected to a resistance of 40 MΩ, under low pressure of 2.5 kPa and high pressure of 25 kPa. Stability measurement at 5 Hz under (c) low pressure of 2.5 kPa and (d) high pressure of 25 kPa.

current in Fig. S11 in the ESM, variation ratio is defined as the difference between the maximum and minimum values divided by the average value. The variation ratios for both low and high applied pressures are less than 5.5% (Table S2 in the ESM), indicating the excellent output stability of our sensor benefitting by the good flexibility of LDPE foamed plastic and electrostatic charges holding ability of Teflon AF electret.

2.4 Demonstration for detecting low pressure generated by human motion

Benefiting by the high sensitivity under low applied pressure, a sensor with 1-layer of LDPE/Teflon AF piezoelectret and effective size of 2 cm × 2 cm is assembled with a wristband to detect low pressure signal generated by human pulse, as shown in Figs. 4(a) and 4(b) as well as Movie ESM1. The measured pulse wave from the sensor is processed with a current amplifier and a data acquisition (DAQ) system and then shown in a personal computer. Like other electromechanical sensors for human pulse detection, a proper preload is needed to exert on the sensor, which can be realized by adjusting the tension between the wristband and the wrist. For the current amplifier, the filter frequency is selected as 10 Hz and the sensitivity is set as 1 nA/V. The data acquisition card can convert the analog signal from the current amplifier into digital signal, and the sampling rate is 50 Hz to reduce the influence of background noise. Finally, the measured pulse wave can be displayed and stored with the LabVIEW software. The pulse waves of tester A (male, 33-year-old) and tester B (male, 35-year-old) are illustrated in Figs. 4(c) and 4(d). Typical characteristic peaks of human pulse are captured for the two testers. These feature peaks are labelled as initially positive (A-wave), early negative (B-wave), reincreasing (C-wave), late redecreasing (D-wave), and diastolic positive (E-wave) [31, 38], respectively. Based on time intervals between all adjacent peak values of A-waves (Table S3 in the ESM), the heartbeat rates of the testers are obtained, which are about 80 and 81 times/min, consisting with the normal heartbeat rate of healthy young men (60–100 times/min) [31]. The peak values of A-wave are very close for tester A and tester B. However, the negative peak values of B-wave present significant differences, and the value of tester A is larger than that of tester B. In addition, the consistency of the negative peak value of B-wave of tester A is significantly better than that of tester B, which indicates that the heartbeat of tester A is more regular.

2.5 Demonstration for detecting high pressure generated by human motion

High pressure signal generated by human motion like sitting can also be detected by our sensor because of the good softness and flexibility. Figure 5(a) illustrates the schematic diagram of a wireless sensing system based on 4 pixels sensors array, measuring circuit, and a designed App. The wireless system is assembled with a chair for wirelessly monitoring the human sitting information with such a "smart chair". In specific, sensors labelled as S1, S2, and S3 locate on the seat of the chair with a distance between each other of 13 cm, and sensor labelled as S4 is on the seat back, as shown in Fig. 5(b). The measured signals generated by different postures are processed by an Arduino board and then sent to the App on smartphone through Wi-Fi network and a cloud server. Finally, the sitting information including defined sitting statuses and cumulative duration can be displayed on the App in real time. As shown in the insert of Fig. 5(b) and Fig. S12 in the ESM, the measuring circuit is mainly composed of the Arduino board (Nano 33 IoT) powered by a mini mobile power supply (SIKAI, 29 g, 5 V, 1,200 mAh), and four analog pins (A0, A1, A2, and A3) are assigned to sensors of S1, S2, S3, and S4. Moreover, four resistors of 10 MΩ are connected in parallel at each end of the four sensors to reduce the background noise.

In this demonstration, five defined sitting statuses (Table S4 in the ESM) are labelled as "Nobody (nobody sitting on the chair)", "Right (sitting on the right of the seat)", "Left (sitting on the left of the seat)", "Back (leaning against the seat back)", and "Correct (sitting at correct status)". The outputs from each sensor are converted into "1" or "0" digital signal via the flowchart in Fig. S13 in the ESM. The conversion process is successfully verified in Fig. S14 in the ESM. Then, we can define the output state of four sensors to map the five defined sitting statuses. Typically, "0000", "1100", "0110", "1110", and "1111" are for "Nobody", "Right", "Left", "Correct", and "Back", respectively, as shown in Table S4 in the ESM. For example, "1" digital signals are detected from S1 and S2 at the same time, and we label the state of four sensors as

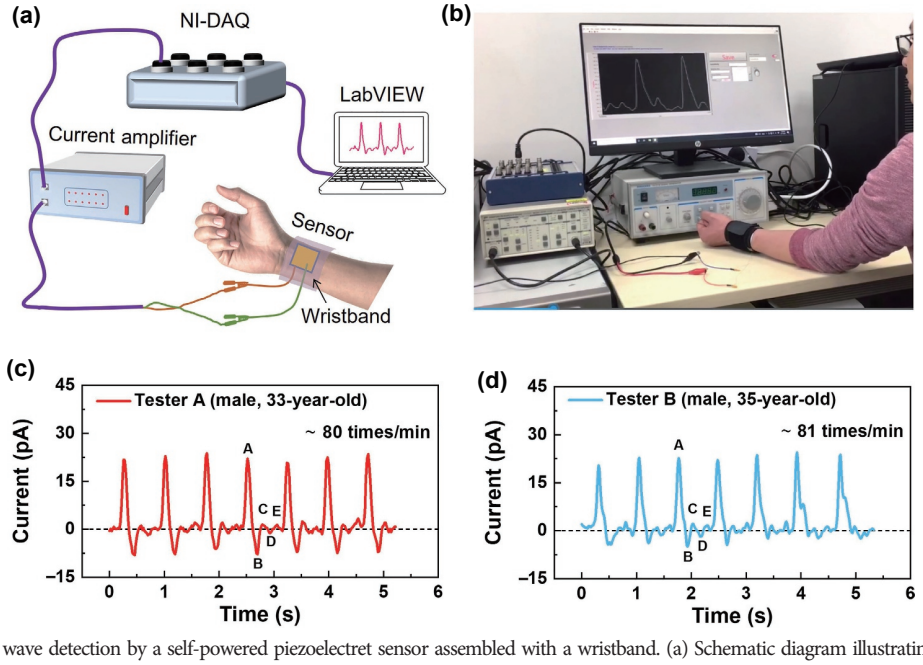

Figure 4 Human pulse wave detection by a self-powered piezoelectret sensor assembled with a wristband. (a) Schematic diagram illustrating the testing system. (b) Photo of the testing system. (c) Measured human pulse waves from tester A. (d) Measured human pulse waves from tester B.

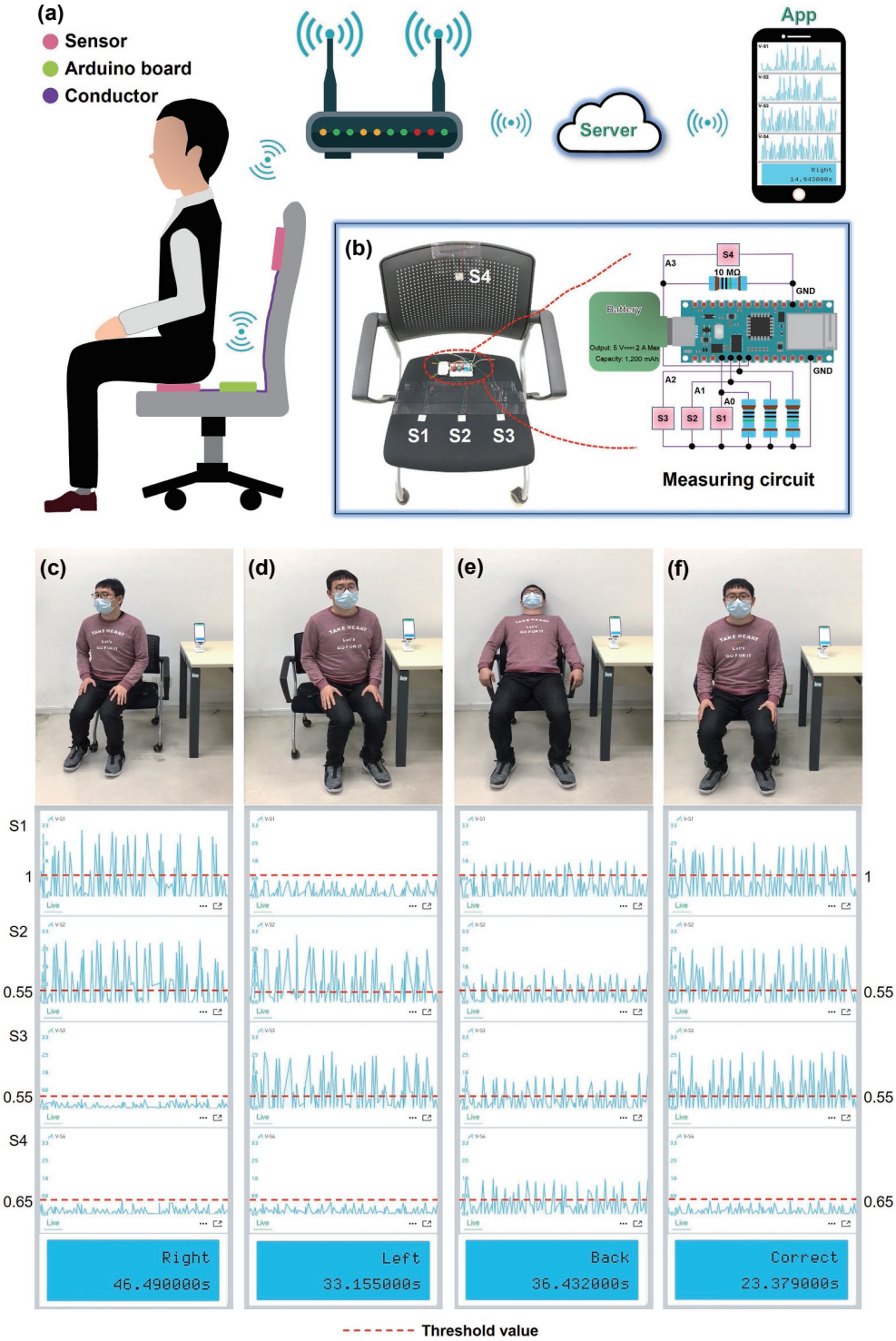

Figure 5 Smart chair based on self-powered sensors array for wirelessly detecting sitting information in real time. (a) Schematic diagram illustrating the working process of the smart chair based on self-powered sensors array. (b) Photo of the smart chair, with insert showing the measuring circuit. Detected sitting information: (c) sitting on the right of the seat (Right), (d) sitting on the left of the seat (Left), (e) leaning against the seat back (Back), and (f) sitting at correct status (Correct).

"1100", which indicates that the tester is sitting on the right of the seat ("Right"), and corresponding cumulative duration will display on the smartphone in real time. As shown in Figs. 5(c)–5(f) and Movie ESM2, the detailed outputs of each sensor under four sitting statuses and the corresponding cumulative durations of each status are successfully monitored, which are 46.490 s for "Right", 33.115 s for "Left", 36.432 s for "Back", and 23.379 s for "Correct", respectively. The threshold output values recorded by Arduino board are used for defining "1" or "0" for each sensor. The threshold values for each sensor in the array are individually set to be larger than the background noise, which are 1, 0.55, 0.55, and 0.65 for S1, S2, S3, and S4, respectively. Moreover, Fig. S15 in the ESM shows the tested results when nobody sits on the chair. The sitting status of "Nobody" is also successfully recognized.

3 Conclusions

In summary, a self-powered flexible piezoelectret sensor based on LDPE foamed plastic garbage with equivalent piezoelectric coefficient d_{33} as high as ~ 1,100 pC/N is proposed in this work and its excellent output abilities are also proved. Demonstrations in detecting both low- and high-pressure signals generated by human motions with our sensor are successfully realized: (i)

Human pulse waves from two testers are measured by a sensor integrated with a wristband and the pulse wave details are clearly shown and compared; (ii) various sitting information is wirelessly monitored in real time by a smart chair based on 4 pixels sensors array. Our work verifies one of the feasibilities of realizing the concept of "turning garbage into treasure".

4 Experimental sections

4.1 Fabrication of the sensor

The detailed fabrication steps are indicated in Fig. S1 in the ESM, with 8 steps. Step 1—Preparing Teflon AF solution: Teflon AF powder (Teflon®, AF1600, Dupont) was dissolved into a solvent (FC-43, 3M) at a concentration of 3 wt.% for 6 h at 70 °C and was stirred at a speed of 300–400 r/min [37]. Step 2: Adhering Al electrode (50 μm-thick Al tape) on one surface of LDPE film and then fixing the laminated films on a glass piece. Step 3: Dropping specific amount of Teflon AF solution on the LDPE surface without electrode. Step 4: Placing the as-fabricated sample in lab environment for 15 min to make the Teflon AF solution fully penetrate into the air bubbles of LDPE. Step 5: Spin coating the as-fabricated sample at 100 r/min for 1 min. Step 6: Heat curing the as-fabricated sample at 100 °C for 4 h. Step 7: Corona charging the fabricated LDPE/Teflon AF piezoelectret, with charging voltage of −15 kV and charging time of 5 min. Step 8: Adhering another Al electrode (50 μm-thick Al tape) to form a sensor. In fact, the glue layer can be regarded as a thin dielectric layer between the conductive Al and LDPE piezoelectret, and the glue layer has ignorable effect on the outputs of the sensors.

4.2 Characterization

The morphology of the samples was examined by a high-resolution field emission scanning electron microscope (Sigma FE-SEM, Zeiss Corporation, Germany). The surface potential of the samples was measured with an electrostatic voltmeter (Trek 347). The output current signals from the sensor were recorded using a Stanford low-noise current preamplifier (Model SR570) and NI USB 6341. The regular mechanical stimulation applied on the samples was provided by a Modal shaker (JZK-10) controlled by a YE1311 sweep signal generator and a YE5872A power amplifier. The force signals applied on the sensor were measured by a force gauge (Mark-10, M7-10). The study protocol was thoroughly reviewed and approved by the ethical committee of University of Macau (approval number BSERE21-APP022-FST). Informed signed consent for the volunteer tests was obtained from the volunteers prior to their participation in this study.

Acknowledgements

We acknowledge the funding support from the Science and Technology Development Fund, Macau SAR (FDCT) (Nos. 0059/2021/AFJ, 0040/2021/A1, 0018/2019/AKP, and SKL-IOTSC(UM)-2021-2023), and the Start Research Grant from University of Macau (No. SRG2021-00001-FST).

Electronic Supplementary Material: Supplementary material (the detailed fabrication process of the sensor, EDS of LDPE raw material, basic properties of the sensor, the method to measure the equivalent d_{33} coefficient, schematic diagrams of corona charging and electrical output performance test system, specifications of the key equipment, optical photos of sensors with effective size of 2 cm × 2 cm, 3 cm × 3 cm, 4 cm × 4 cm, and 5 cm × 5 cm, sensors with 1-layer, 2-layers, 3-layers, and 4-layers of LDPE/Teflon AF piezoelectret, further details of current, calculation details of the variation ratio of current, more details for calculating the heartbeat rates, image for Arduino board and its peripheral circuits, relationship between sensor states and sitting statuses, flowchart of the smart chair for wirelessly detecting sitting information in real time, verification of conversion of the detected signals to high and low levels, and detected sitting information) is available in the online version of this article at https://doi.org/10.1007/s12274-022-4766-8.

References

[1] Borrelle, S. B.; Ringma, J.; Law, K. L.; Monnahan, C. C.; Lebreton, L.; McGivern, A.; Murphy, E.; Jambeck, J.; Leonard, G. H.; Hilleary, M. A. et al. Predicted growth in plastic waste exceeds efforts to mitigate plastic pollution. *Science* **2020**, *369*, 1515–1518.

[2] Law, K. L.; Narayan, R. Reducing environmental plastic pollution by designing polymer materials for managed end-of-life. *Nat. Rev. Mater.* **2022**, *7*, 104–116.

[3] Worm, B.; Lotze, H. K.; Jubinville, I.; Wilcox, C.; Jambeck, J. Plastic as a persistent marine pollutant. *Annu. Rev. Environ. Resour.* **2017**, *42*, 1–26.

[4] Bauer, S.; Gerhard-Multhaupt, R.; Sessler, G. M. Ferroelectrets: Soft electroactive foams for transducers. *Phys. Today* **2004**, *57*, 37–43.

[5] The Guardian. *Amazon's Plastic Waste Soars by A Third During Pandemic, Oceana Report Finds* [Online]. 2021. https://www.theguardian.com/environment/2021/dec/15/amazon-plastic-waste-soars-by-a-third-amid-pandemic-finds-oceana-report (accessed Jun 20, 2022).

[6] Chen, H. L.; Nath, T. K.; Chong, S.; Foo, V.; Gibbins, C.; Lechner, A. M. The plastic waste problem in Malaysia: Management, recycling and disposal of local and global plastic waste. *SN Appl. Sci.* **2021**, *3*, 437.

[7] Hu, H.; Zhu, W. J.; Li, D. S.; Qu, Y. Waterproof and low-cost piezoelectrets with high piezoelectric responses. *J. Phys. D: Appl. Phys.* **2021**, *54*, 415502.

[8] Ma, X. C.; Zhang, X. Q.; Fang, P. Flexible film-transducers based on polypropylene piezoelectrets: Fabrication, properties, and applications in wearable devices. *Sens. Actuat. A:Phys.* **2017**, *256*, 35–42.

[9] Moreira, M. M. A. C.; Soares, I. N.; Assagra, Y. A. O.; Sousa, F. S. I.; Nordi, T. M.; Dourado, D. M.; Gounella, R. H.; Carmo, J. P.; Altafim, R. A. C.; Altafim, R. A. P. Piezoelectrets: A brief introduction. *IEEE Sens. J.* **2021**, *21*, 22317–22328.

[10] Zhang, M.; Zuo, X.; Yang, T. Q.; Zhang, X. Q. Research progress of piezoelectrets based micro-energy harvesting. *Acta Phys. Sin.* **2020**, *69*, 247701.

[11] Chen, L.; Cao, J. L.; Li, G. L.; Fang, P.; Gong, X. S.; Zhang, X. Q. Property assessment and application exploration for layered polytetrafluoroethylene piezoelectrets. *IEEE Sens. J.* **2019**, *19*, 11262–11271.

[12] Mo, X. W.; Zhou, H.; Li, W. B.; Xu, Z. S.; Duan, J. J.; Huang, L.; Liu, B.; Zhou, J. Piezoelectrets for wearable energy harvesters and sensors. *Nano Energy* **2019**, *65*, 104033.

[13] Wang, B.; Liu, C.; Xiao, Y. J.; Zhong, J. W.; Li, W. B.; Cheng, Y. L.; Hu, B.; Huang, L.; Zhou, J. Ultrasensitive cellular fluorocarbon piezoelectret pressure sensor for self-powered human physiological monitoring. *Nano Energy* **2017**, *32*, 42–49.

[14] Baek, S.; Lee, Y.; Baek, J.; Kwon, J.; Kim, S. Lee, S.; Strunk, K. P.; Stehlin, S.; Melzer, C.; Park, S. M. et al. Spatiotemporal measurement of arterial pulse waves enabled by wearable active-matrix pressure sensor arrays. *ACS Nano* **2022**, *16*, 368–377.

[15] Feng, H. Q.; Zhao, C. C.; Tan, P. C.; Liu, R. P.; Chen, X.; Li, Z. Nanogenerator for biomedical applications. *Adv. Heal. Mater.* **2018**, *7*, 1701298.

[16] Persano, L.; Dagdeviren, C.; Su, Y. W.; Zhang, Y. H.; Girardo, S.; Pisignano, D.; Huang, Y. G.; Rogers, J. A. High performance piezoelectric devices based on aligned arrays of nanofibers of poly(vinylidenefluoride-co-trifluoroethylene). *Nat. Commun.* **2013**, *4*, 1633.

[17] Chang, C.; Tran, V. H.; Wang, J. B.; Fuh, Y. K.; Lin, L. W. Direct-write piezoelectric polymeric nanogenerator with high energy conversion efficiency. *Nano Lett.* **2010**, *10*, 726–731.
[18] Zhang, P. P.; Chen, Y. H.; Guo, Z. H.; Guo, W. B.; Pu, X.; Wang, Z. L. Stretchable, transparent, and thermally stable triboelectric nanogenerators based on solvent-free ion-conducting elastomer electrodes. *Adv. Funct. Mater.* **2020**, *30*, 1909252.
[19] Zhu, G.; Yang, W. Q.; Zhang, T. J.; Jing, Q. S.; Chen, J.; Zhou, Y. S.; Bai, P.; Wang, Z. L. Self-powered, ultrasensitive, flexible tactile sensors based on contact electrification. *Nano Lett.* **2014**, *14*, 3208–3213.
[20] Das, P. S.; Chhetry, A.; Maharjan, P.; Rasel, M. S.; Park, J. Y. A laser ablated graphene-based flexible self-powered pressure sensor for human gestures and finger pulse monitoring. *Nano Res.* **2019**, *12*, 1789–1795.
[21] Lei, H.; Xiao, J.; Chen, Y. F.; Jiang, J. W.; Xu, R. J.; Wen, Z.; Dong, B.; Sun, X. H. Bamboo-inspired self-powered triboelectric sensor for touch sensing and sitting posture monitoring. *Nano Energy* **2022**, *91*, 106670.
[22] Cao, R.; Wang, J. N.; Zhao, S. Y.; Yang, W.; Yuan, Z. Q.; Yin, Y. Y.; Du, X. Y.; Li, N. W.; Zhang, X. L.; Li, X. Y. et al. Self-powered nanofiber-based screen-print triboelectric sensors for respiratory monitoring. *Nano Res.* **2018**, *11*, 3771–3779.
[23] Zhang, M. C.; Zhao, M. Y.; Jian, M. Q.; Wang, C. Y.; Yu, A. F.; Yin, Z.; Liang, X. P.; Wang, H. M.; Xia, K. L.; Liang, X. et al. Printable smart pattern for multifunctional energy-management E-textile. *Matter* **2019**, *1*, 168–179.
[24] Kim, H. J.; Kim, J. H.; Jun, K. W.; Kim, J. H.; Seung, W. C.; Kwon, O. H.; Park, J. Y.; Kim, S. W.; Oh, I. K. Silk nanofiber-networked bio-triboelectric generator: Silk Bio-TEG. *Adv. Energy Mater.* **2016**, *6*, 1502329.
[25] Guo, Y. B.; Zhang, X. S.; Wang, Y.; Gong, W.; Zhang, Q. H.; Wang, H. Z.; Brugger, J. All-fiber hybrid piezoelectric-enhanced triboelectric nanogenerator for wearable gesture monitoring. *Nano Energy* **2018**, *48*, 152–160.
[26] Li, S.; Zhang, Y.; Wang, Y. L.; Xia, K. L.; Yin, Z.; Wang, H. M.; Zhang, M. C.; Liang, X. P.; Lu, H. J.; Zhu, M. J. et al. Physical sensors for skin-inspired electronics. *InfoMat* **2020**, *2*, 184–211.
[27] Shi, Y. X.; Wang, F.; Tian, J. W.; Li, S. Y.; Fu, E. G.; Nie, J. H.; Lei, R.; Ding, Y. F.; Chen, X. Y.; Wang, Z. L. Self-powered electro-tactile system for virtual tactile experiences. *Sci. Adv.* **2021**, *7*, eabe2943.
[28] Yang, P.; Shi, Y. X.; Li, S. Y.; Tao, X. L.; Liu, Z. Q.; Wang, X. L.; Wang, Z. L.; Chen, X. Y. Monitoring the degree of comfort of shoes in-motion using triboelectric pressure sensors with an ultrawide detection range. *ACS Nano* **2022**, *16*, 4654–4665.
[29] Wang, X. L.; Shi, Y. X.; Yang, P.; Tao, X. L.; Li, S. Y.; Lei, R.; Liu, Z. Q.; Wang, Z. L.; Chen, X. Y. Fish-wearable data snooping platform for underwater energy harvesting and fish behavior monitoring. *Small* **2022**, *18*, 2107232.
[30] Zhong, J. W.; Zhong, Q. Z.; Zang, X. N.; Wu, N.; Li, W. B.; Chu, Y.; Lin, L. W. Flexible PET/EVA-based piezoelectret generator for energy harvesting in harsh environments. *Nano Energy* **2017**, *37*, 268–274.
[31] Wu, N.; Cheng, X. F.; Zhong, Q. Z.; Zhong, J. W.; Li, W. B.; Wang, B.; Hu, B.; Zhou, J. Cellular polypropylene piezoelectret for human body energy harvesting and health monitoring. *Adv. Funct. Mater.* **2015**, *25*, 4788–4794.
[32] Chu, Y.; Zhong, J. W.; Liu, H. L.; Ma, Y.; Liu, N.; Song, Y.; Liang, J. M.; Shao, Z. C.; Sun, Y.; Dong, Y. et al. Human pulse diagnosis for medical assessments using a wearable piezoelectret sensing system. *Adv. Funct. Mater.* **2018**, *28*, 1803413.
[33] Zhong, J. W.; Ma, Y.; Song, Y.; Zhong, Q. Z.; Chu, Y.; Karakurt, I.; Bogy, D. B.; Lin, L. W. A flexible piezoelectret actuator/sensor patch for mechanical human-machine interfaces. *ACS Nano* **2019**, *13*, 7107–7116.
[34] Fang, P.; Ma, X. C.; Li, X. X.; Qiu, X. L.; Gerhard, R.; Zhang, X. Q.; Li, G. L. Fabrication, structure characterization, and performance testing of piezoelectret-film sensors for recording body motion. *IEEE Sens. J.* **2018**, *18*, 401–412.
[35] Li, X. X.; Zhuo, Q. F.; Zhang, X.; Samuel, O. W.; Xia, Z. Y.; Zhang, X. Q.; Fang, P.; Li, G. L. FMG-based body motion registration using piezoelectret sensors. In *Proceedings of the 38th Annual International Conference of the IEEE Engineering in Medicine and Biology Society (EMBC)*, Orlando, FL, USA, 2016, pp 4626–4629.
[36] Chen, S. W.; Wu, N.; Ma, L.; Lin, S. Z.; Yuan, F.; Xu, Z. S.; Li, W. B.; Wang, B.; Zhou, J. Noncontact heartbeat and respiration monitoring based on a hollow microstructured self-powered pressure sensor. *ACS Appl. Mater. Interfaces* **2018**, *10*, 3660–3667.
[37] Zhong, J. W.; Li, Z. Y.; Takakuwa, M.; Inoue, D.; Hashizume, D.; Jiang, Z.; Shi, Y. J.; Ou, L. X.; Nayeem, O. G.; Umezu, S. et al. Smart face mask based on an ultrathin pressure sensor for wireless monitoring of breath conditions. *Adv. Mater.* **2022**, *34*, 2107758.
[38] Yang, J.; Chen, J.; Su, Y. J.; Jing, Q. S.; Li, Z. L.; Yi, F.; Wen, X. N.; Wang, Z. N.; Wang, Z. L. Eardrum-inspired active sensors for self-powered cardiovascular system characterization and throat-attached anti-interference voice recognition. *Adv. Mater.* **2015**, *27*, 1316–1326.